Effects of eddy shocklets on the segregation and evaporation of droplets in highly compressible shear layers

Cite as: AIP Advances **9**, 125101 (2019); https://doi.org/10.1063/1.5125121
Submitted: 20 August 2019 • Accepted: 11 November 2019 • Published Online: 02 December 2019

Zhaoxin Ren, Bing Wang, Fan Zhang, et al.

Effects of eddy shocklets on the segregation and evaporation of droplets in highly compressible shear layers

Cite as: AIP Advances 9, 125101 (2019); doi: 10.1063/1.5125121
Submitted: 20 August 2019 • Accepted: 11 November 2019 •
Published Online: 2 December 2019

Zhaoxin Ren,[1] Bing Wang,[2,a)] Fan Zhang,[3] and Longxi Zheng[1]

AFFILIATIONS

[1]School of Power and Energy, Northwestern Polytechnical University, Xi'an 710072, China
[2]School of Aerospace Engineering, Tsinghua University, Beijing 100084, China
[3]China Academy of Launch Vehicle Technology, Beijing 100076, China

[a)]wbing@tsinghua.edu.cn

ABSTRACT

Numerical studies of droplet-laden spatially developing shear layers are conducted with a high convective Mach number (M_c = 1.0), in which a high-order hybrid weighted essentially nonoscillatory scheme is used for the turbulence as well as shock capturing. The evaporating droplets are tracked as point mass in the Lagrangian manner, and the two-way coupling between the flow and droplets is considered by adding the source terms to the governing equations of the gas-phase. This research focuses on the preferential concentration of droplets and the interactions between droplets and eddy shocklets in the shear layers with high flow compressibility and analyzes the underlying mechanisms of momentum and thermal response behaviors of droplets to eddy shocklets. The segregation of droplets exhibits the strongest spatial preference in the highly compressible shearing vortices, and droplets tend to accumulate as stripes behind the shocklets, associated with the coherent structures. The high flow compressibility results in the strong spatiotemporal variations of pressure and temperature, and the distributions of the expansion zones with low temperature and the compression zones with high temperature occur alternately in the shear layer. The relaxation response behaviors of the droplets to the change of momentum and thermal features of the surrounding carrier gas result in the delay of droplet evaporation in the high temperature region and then the enhancement of droplet-vapors in the low temperature region. The present observations can be ascribed to the interactions between the dispersed droplets and the distributed eddy shocklets in the shear flows with high compressibility.

I. INTRODUCTION

The multiphase compressible/supersonic flows laden with dispersed droplets occur commonly in various natural and engineering applications, such as spray combustion of liquid fuel in engines, atmospheric dispersion of pollutants, and so on. These research areas involve the transportation and dispersion of the dispersed phase as well as the droplet evaporation in the carrier phase, which are fundamental topics in the research of multiphase flow and combustion.[1] In particular, the combustion in a high-speed propulsion system such as supersonic combustion ramjets (scramjets) often faces flow compressibility. Both the rotational motion of fluid and the flow compressibility are found to become important as turbulence is highly compressible in supersonic flows. The dynamics of turbulence become complicated due to these influences and result in the generation or destruction of turbulent kinetic energy. In particular, the shock waves can amplify the vorticity and turbulent kinetic energy. Furthermore, the dilatation fields are changed obviously in the presence of eddy shocklets[2] formed in the supersonic turbulent flows and the turbulent kinetic energy tends to dissipate at smaller wave numbers, compared with subsonic flows. The flow characteristics could result in the more complex problems of supersonic flows laden with droplets. Therefore, it is important to consider the physics and mechanisms of the interphase interactions between

droplets and compressible flows, and the research could be used to improve the design and operation of the combustion chamber of scramjets.

The velocity of sprayed droplets is affected by the local gas turbulence due to the momentum transfer between the gas and liquid phases. The momentum response of the droplet to the local flow depends on its inertia, and the particle Stokes number (St) can be used to describe the response characteristic. St is the ratio of the droplet acceleration time to the time characterizing the flow dynamics of carrier phase. There have been intensive investigations in experiments and numerical simulations[3,4] on the dispersion and segregation of particles in the incompressible turbulent flows. The particles have different dispersion features in the carrier flow due to the momentum response behavior. It was observed that the particles concentrate preferentially in turbulence and the particle spatial distribution exhibits strong uniformity. The preferential segregation of inertial particles was first observed in the 1960s for the research of turbulent pipe flow,[5] and the researchers found that the turbulent fluctuations were enhanced by the concentrated particles. Similar results were observed in the free shear layer,[6] plane turbulent mixing layer,[7] and round jet.[8] The turbulent structures of carrier flow have significant effects on the clustering features of inertial particles. It was observed that the particles with low density couple in the regimes with high vorticity,[9] while the particles with high density are found to be expelled by the motion of vortices,[10] and they preferentially collect in the peripheries of vortices. The above results are from the studies on the homogeneous isotropic flow. Similar conclusions were found in the numerical studies of anisotropic turbulence, such as channel flow[11] and shear flow.[12] Furthermore, Dodd and Ferrante[13] presented a novel analysis of how the homogeneous turbulence interacts with the suspended droplets and provided new insights into how turbulence affects the motion of the droplets, associated with their shape and size.

Most of the previous investigation analyzed the dispersion features of particles in incompressible turbulent flows. Compressible turbulent flow has also been researched extensively, such as the shock-turbulence interaction[14] and compressible isotropic turbulence.[15] However, only recently, some effort has been made to investigate the dispersion of particles in compressible flows and the effects of flow compressibility were considered. In particular, Samimy and Lele[16] analyzed the compressible free shear layers laden with particles by the two-dimensional numerical simulation and the convective Mach number (M_c) was varied from 0.2 to 0.6. The dispersion features were found to be similar to those in the incompressible flows. Mashayek and Jaberi[17] studied the isotropic turbulence and the turbulent Mach number (M_t) was smaller than 0.2. The M_t is the ratio of the root-mean-square of the fluctuating velocity to the mean value of the sound speed. The solid particles were found to distribute in the flow regions with high strain rates, which were consistent with the previous conclusions for the incompressible flow. This is mainly because the turbulence had weak flow compressibility and the eddy shocklets were not formed. Olla[18] analyzed the clustering of particles by a one-dimensional (1D) mathematical model and found that the inertial particles generally concentrate in the area with negative dilatation as they are entrained by the local compressible flow with random velocities. As the flow compressibility increases to form shocklets, these wave structures were found to influence the transportation of particles. Yang *et al.*[19] numerically investigated the unsteady motions of inert particles in a temporally developing homogeneous turbulent flow and the turbulent Mach number, M_t, equals to 1. The light particles tend to form filamentlike structures and the particles with high density accumulate in the neighboring downstream regimes of eddy shocklets. Zhang *et al.*[20] analyzed the effects of compressible turbulence on the dispersions of particles in an isotropic flow by numerical simulations and observed that the particles with high density tend to segregate in the high-density regimes and the particles have the strongest preferential concentration as their Stokes numbers are close to unity. The particles with intermediate and large Stokes numbers are observed to distribute in the flow areas with high vorticity that are in the downstream regions of shocklets. The increase in M_t leads to the enhanced segregation of particles in the high-vorticity regions. This is because the shocklets increase as the M_t increases, which results in the enhancement of vorticity and pressure of the turbulence.

It is noteworthy that there are few studies on the effects of compressible flows on evaporating droplets despite its significance in many physical processes and engineering applications. The previous research has indicated that the eddy shocklets formed in highly compressible flows affect the segregation of particles without heat and mass transfers, which can influence the evaporation process as well as the spatial distribution of vapors. This would further decide the features of ignition and combustion of liquid fuel. The physics for the mass, momentum, and heat transfers from the eddy shocklets to dispersing droplets in a spatially developing flow should be revealed in detail to have a better understanding of spray combustion in supersonic flows.

The aim of this paper is to analyze and discuss the influence of eddy shocklets in supersonic flows with high-speed compressibility on the dispersion and evaporation of fuel droplets (*n*-decane, $C_{10}H_{22}$) via numerical simulation applying a high-order hybrid weighted essentially nonoscillatory (WENO) scheme, with the convective Mach number (M_c) equaling to unity. Emphasis is placed on the effects of the random eddy shocklets on the evaporating droplets and the instantaneous characteristics of heat and mass transfers as the droplets traverse the shocklets. This paper is organized as follows: Section I introduces the background. Section II details the physical models and numerical methods. Section III provides the results and analysis, including the characteristics of carrier flow field, the statistics of the spatial distribution of fuel droplets, and the effects of eddy shocklets on the instantaneous momentum/heat transfer from fluid to droplets. Section IV presents the conclusions.

II. GOVERNING EQUATIONS AND NUMERICAL METHODS

A. Governing equations

For the mathematical model, the motion of evaporating fuel droplets in a supersonic shear layer is considered. The flow is treated as an ideal gas with multispecies (O_2 and N_2). The governing equations for the mass, momentum, and energy conservations and the transport equations of three species ($C_{10}H_{22}$, O_2, and N_2) are solved. The equation of state for the ideal multispecies gas is applied. The

equations are as follows:

$$\frac{\partial \rho}{\partial t} + \frac{\partial}{\partial x_j}(\rho u_j) = S_{\mathrm{m}}, \tag{1}$$

$$\frac{\partial}{\partial t}(\rho u_i) + \frac{\partial}{\partial x_j}(\rho u_i u_j + P\delta_{ij} - \tau_{ij}) = S_{\mathrm{F},i}, \tag{2}$$

$$\frac{\partial}{\partial t}(\rho e_{\mathrm{t}}) + \frac{\partial}{\partial x_j}((\rho e_{\mathrm{t}} + P)u_j - u_i\tau_{ij} - q_j) = S_{\mathrm{Q}}, \tag{3}$$

$$\frac{\partial}{\partial t}(\rho Y_k) + \frac{\partial}{\partial x_j}(\rho Y_k u_j) + \frac{\partial}{\partial x_j}\left(\rho Y_k\left(V_{k,j} + V_j^{\mathrm{c}}\right)\right) = S_{Y_k}, \tag{4}$$

$$P = \rho R T \sum_{k=1}^{N_S} \frac{Y_k}{W_k}, \tag{5}$$

where ρ, u_i, T, and P are density, velocity, temperature, and pressure, respectively. τ_{ij} and V_j^c are the Newtonian viscous stress tensor and the correction velocity, respectively. Y_k is the mass fraction of the kth species. N_S is the total number of species, and W_k is the molecule weight of the kth species. R is the universal gas constant. e_{t} is the total energy, i.e., kinetic energy plus internal (containing chemical) energy, which is defined as

$$e_{\mathrm{t}} = \sum_{k=1}^{N_S} Y_k\left(\int_{T_{\mathrm{ref}}}^{T} c_{p,k}\mathrm{d}T + h_{f,k}^0\right) - \frac{P}{\rho} + \frac{u_i u_i}{2}, \tag{6}$$

where $c_{p,k}$ is the specific heat capacity at a constant pressure and $h_{f,k}^0$ is the specific chemical formation enthalpy at the reference temperature, T_{ref}. The $c_{p,k}$ are calculated by a fifth-order polynomial.[21] The kinetic theory[22] is applied for the transportation and thermodynamic properties of the gaseous mixture. The intermolecular forces are calculated based on the Lennard-Jones potentials of each chemical species. The modified Eucken model is applied for calculating the heat conductivity. The Chapman-Enskog theory is used for computing the binary diffusion coefficient and the dynamic viscosity. The source terms, S_{m}, $S_{\mathrm{F},i}$, and S_{Q}, which describe the interactions of mass, momentum, and energy between the liquid and gas phases, are modeled by amounting the total number of droplets, N, existing in the local grid for the simulation of the gas phase,

$$S_m = -\frac{1}{\Delta V}\sum_N (\dot{m}_{\mathrm{d}}), \tag{7a}$$

$$S_{\mathrm{F},i} = -\frac{1}{\Delta V}\sum_N (F_{\mathrm{d},i} + \dot{m}_{\mathrm{d}} u_{\mathrm{d},i}), \tag{7b}$$

$$S_{\mathrm{Q}} = -\frac{1}{\Delta V}\sum_N \left(Q_{\mathrm{d}} + \dot{m}_{\mathrm{d}}\left(\frac{u_{\mathrm{d},i}u_{\mathrm{d},i}}{2} + h_{\mathrm{V,sf}}\right)\right), \tag{7c}$$

$$S_{Y_k} = \begin{cases} -\frac{1}{\Delta V}\sum\limits_N (\dot{m}_{\mathrm{d}}) & \text{for fuel} \\ 0 & \text{for other species,} \end{cases} \tag{7d}$$

where m_{d} is the mass of the droplet and $\dot{m}_{\mathrm{d}}$ is the mass transfer rate. $u_{\mathrm{d},i}$ is the velocity of the droplet. $h_{\mathrm{V,sf}}$ is the vapor enthalpy at the droplet surface. ΔV is the volume of the grid. $F_{\mathrm{d},i}$ and Q_{d} are drag force and the convective heat transfer acting on the droplet, respectively.

The droplet phase contains many discrete droplets dispersing in the supersonic flows. The single droplet is tracked individually. The droplets are sparsely distributed, and each droplet is not affected by the others in which the droplet-droplet interaction and coalescence are neglected. The inner temperature distribution of each droplet is assumed to be uniform. Only the drag force on the droplet is considered due to the high-density ratio of liquid to gas phases. Therefore, the droplet position ($x_{\mathrm{d},i}$), velocity ($u_{\mathrm{d},i}$), temperature (T_{d}), and mass (m_{d}), can be written as

$$\frac{\mathrm{d}x_{\mathrm{d},i}}{\mathrm{d}t} = u_{\mathrm{d},i}, \tag{8}$$

$$\frac{\mathrm{d}u_{\mathrm{d},i}}{\mathrm{d}t} = \frac{F_{\mathrm{d}}}{m_{\mathrm{d}}} = \left(\frac{f_{\mathrm{F}}(\mathrm{Re}_{\mathrm{d}})}{\tau_{\mathrm{d}}}\right)(u_{i@\mathrm{d}} - u_{\mathrm{d},i}), \tag{9}$$

$$\frac{\mathrm{d}T_{\mathrm{d}}}{\mathrm{d}t} = \frac{Q_{\mathrm{d}} + \dot{m}_{\mathrm{d}}L_{\mathrm{V}}}{m_{\mathrm{d}}c_{\mathrm{L}}} = \left(\frac{f_{\mathrm{Q}}}{\tau_{\mathrm{d}}}\right)\left(\frac{\mathrm{Nu}}{3\,\mathrm{Pr}}\right)\left(\frac{c_p}{c_{\mathrm{L}}}\right)(T_{@\mathrm{d}} - T_{\mathrm{d}}) + \left(\frac{\dot{m}_{\mathrm{d}}}{m_{\mathrm{d}}}\right)\frac{L_{\mathrm{V}}}{c_{\mathrm{L}}}, \tag{10}$$

$$\frac{\mathrm{d}m_{\mathrm{d}}}{\mathrm{d}t} = \dot{m}_{\mathrm{d}} = -m_{\mathrm{d}}\left(\frac{1}{\tau_{\mathrm{d}}}\right)\left(\frac{\mathrm{Sh}}{3\mathrm{Sc}}\right)\mathrm{In}(1 + B_{\mathrm{M}}), \tag{11}$$

where $u_{i@\mathrm{d}}$ and $T_{@\mathrm{d}}$ are the fluid velocity and temperature seen by the droplet at its position. c_p is the specific heat of the mixture gas (vapor and air), and c_{L} and L_{V} are the specific heat of the liquid phase and the latent heat of fuel vapor at T_{d}, respectively. The momentum response time, τ_{d}, is as follows:

$$\tau_{\mathrm{d}} = \frac{\rho_{\mathrm{d}} d_{\mathrm{d}}^2}{18\mu}, \tag{12}$$

where d_{d} is the droplet diameter. The correction function for the drag force, $f_F(\mathrm{Re}_{\mathrm{d}})$, is

$$f_{\mathrm{F}}(\mathrm{Re}_{\mathrm{d}}) = \frac{\mathrm{Re}_{\mathrm{d}}}{24}\left(\frac{24}{\mathrm{Re}_{\mathrm{d}}}\left(1 + 0.15\,\mathrm{Re}_{\mathrm{d}}^{0.687}\right) + \frac{0.42}{1 + 42\,500\,\mathrm{Re}_{\mathrm{d}}^{-1.16}}\right) \text{ for } \mathrm{Re}_{\mathrm{d}} < 2 \times 10^5. \tag{13}$$

The droplet Reynolds number, Re_{d}, is $\mathrm{Re}_{\mathrm{d}} = |u_i - u_{\mathrm{d},i}|d_{\mathrm{d}}/\nu$. The Prandtl and Schmidt numbers are $\mathrm{Pr} = \mu c_p/\lambda$ and $\mathrm{Sc} = \mu/\rho D$, respectively. The Nusselt (Nu) and Sherwood (Sh) numbers for the heat and mass transfers are

$$\mathrm{Nu} = 2 + 0.552\,\mathrm{Re}_{\mathrm{d}}^{1/2}\mathrm{Pr}^{1/3} \text{ and } \mathrm{Sh} = 2 + 0.552\,\mathrm{Re}_{\mathrm{d}}^{1/2}\mathrm{Sc}^{1/3}. \tag{14}$$

The evaporation rate of a single droplet is based on the mass transfer number, $B_{\mathrm{M}} = (Y_{\mathrm{sf}} - Y_{\mathrm{V}})/(1 - Y_{\mathrm{sf}})$. Here, Y_{V} is the mass fraction of vapor far from the droplet. Y_{sf} is the fuel vapor mass fraction at the droplet interface, which depends on the surface molar fraction (χ_{sf}) from a nonequilibrium evaporation model,[23]

$$Y_{\mathrm{sf}} = \frac{\chi_{\mathrm{sf}}}{\chi_{\mathrm{sf}} + (1 - \chi_{\mathrm{sf}})W/W_{\mathrm{V}}}, \tag{15a}$$

$$\chi_{\mathrm{sf}} = \frac{P_{\mathrm{atm}}}{P}\exp\left(\frac{L_{\mathrm{V}}}{R/W_{\mathrm{V}}}\left(\frac{1}{T_{\mathrm{B,L}}} - \frac{1}{T_{\mathrm{d}}}\right)\right) - \frac{2L_{\mathrm{k}}}{d_{\mathrm{d}}}\beta, \tag{15b}$$

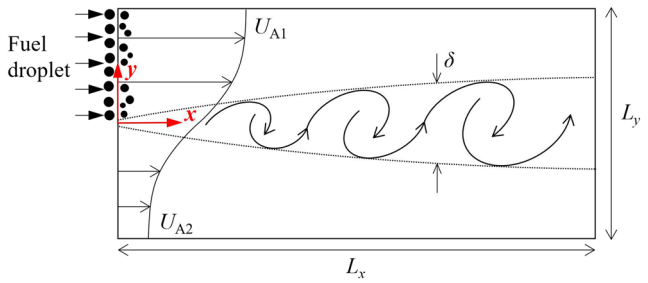

FIG. 1. Schematic of the supersonic shear layer laden with droplets.

$$L_k = \frac{\mu(2\pi T_d(R/W_V))^{1/2}}{ScP}, \tag{15c}$$

where W and W_V are the molecular weight of the gas mixture and the molecular weight of the vapor, respectively. P_{atm} is the atmospheric pressure, and $T_{B,L}$ is the boiling temperature of liquid. L_k is the Knudsen layer thickness for the nonequilibrium evaporation model.

B. Numerical approaches

The governing equations, which include the transport equations of the chemical species and the droplet trajectory equations, are solved via utilizing our in-house simulation code. The code has been utilized to study the compressible multiphase flow and combustion problems[24,25] in the previous research. In particular, the code was validated according to the experiments of the nonreacting supersonic mixing layer and single droplet evaporation. An overall description of the numerical methods is given. A finite difference approach is applied for solving the governing equations. The adaptive central-upwind sixth-order weighted essentially nonoscillatory scheme[26] is applied for reconstructing the numerical fluxes at the grid interfaces, and this scheme ensures the numerical simulations for the turbulent flow with the low dissipation and achieves a good resolution of the flow properties around the shock waves in supersonic flows. A sixth-order symmetric compact difference scheme is applied for the viscous terms. The time-integration is realized by the explicit third-order Runge-Kutta method. For the two-way coupling, the effects of droplets on the local carrier flow are achieved via adding the source terms on the nearest Eulerian grids. A fourth-order Lagrangian interpolation scheme is used to compute the velocity, temperature, pressure, and other physical quantities of the gas-phase at the droplet locations. The new position, velocity, and temperature of the droplet along its trajectory are obtained from a third-order Adams-Bashforth time integration method.

C. Computational setup

The physical model involves two supersonic air streams in the same direction with different velocities U_{A1} and U_{A2}, as depicted in Fig. 1. The velocity ratio of two streams, U_{A2}/U_{A1}, is 0.6. The inflow Mach numbers M_{A1} and M_{A2} are 5.0 and 3.0, and the resulting convective Mach number, M_c, is 1.0. The temperature of the air streams, T_A, is 700 K, and the inflow static pressure, P_A, is 0.1 MPa. The Reynolds number of the inflow, $Re_{\delta 0} = \delta_0 \Delta U_A/\nu_A$, is based on the initial shear layer thickness, δ_0, the velocity difference, ΔU_A, and the kinematic viscosity of air, ν_A, and is 6200. The letters x and y indicate the streamwise and transverse directions, respectively. The inhomogeneous Cartesian grids are applied for the computation, and fine resolution is given around the center of the shear layer according to the stretched meshes in the transverse direction. The finest grid spacing is specified as 50 μm around the shear layer center. The distribution of streamwise velocities at the inflow boundary ($x = 0$) is set as a hyperbolic tangent profile, and a supersonic inlet boundary condition is applied. Transition to turbulence is triggered by introducing the random perturbations to the inflow transverse velocity[27] to promote the flow instabilities. In particular, the random perturbations are added to the transverse component of the inflow velocity based on the most-unstable frequency in the flow field,

$$\begin{aligned} v'(x=0,y) &= (U_1 - U_2)G(y)A\sin(2\pi ft + \xi), \\ u'(x=0,y) &= 0, \end{aligned} \tag{16}$$

where $G(y)$ is Gaussian function, A is the amplitude, and f is the most unstable frequency. The random phase is ξ. The nonreflecting boundary conditions are used at $y = \pm L_y/2$ to reduce the reflection of acoustic waves formed in the shear layer.[28] At $x = L_x$, the supersonic outlet boundary condition is utilized. The n-decane droplets are injected from the high-speed side of the inlet with a width of $L_y/2$, as shown in Fig. 1. The initial droplet size is uniform and the initial droplet velocities keep the same with the local gas velocity. Therefore, the Reynolds number and the Mach number based on the initial slip velocity between droplets and gas are zero. The initial droplet temperature is $T_{d0} = 298.15$ K. The breakup process is not considered in this study, since the Weber number based on the slip velocity between two phases is quite small for the concerned initial conditions. The main physical characteristics of the n-decane droplet are shown in Table I.

III. RESULTS AND DISCUSSION

A. Shocklets in highly compressible shear layers

The high convective Mach number for the present supersonic flow indicates that the eddy-straining time could be the same order

TABLE I. Physical characteristics of the n-decane droplet.

Initial diameter, d_{d0} (μm)	Density, ρ_d (kg m^{-3})	Specific heat, c_L (J kg^{-1} K^{-1})	Liquid boiling temperature at normal pressure, $T_{B,L}$ (K)	Latent heat at $T_{B,L}$, L_V (J K^{-1})
10.0	642.0	2520.5	447.3	279 700.0

with the acoustic time.[29] This feature leads to the strong change of the gas pressure, and the fluctuating amplitude could be the same order with the dynamic pressure during the turnover of the large eddies in the shear layer. The fluctuating pressure results in strong density variations. In particular, the free supersonic stream encounters flow regimes with decreasing velocity and even subsonic regions as the stream is entrained in the shear layer by large eddies. Sometimes these conditions for decreasing to subsonic flows exist coherently between large eddies carrying supersonic and subsonic flows. These flow regimes with intense variations of the Mach numbers were named eddy shocklets in the previous work, and the shocklets develop more prominently on the high-speed side of the mixing layer due to the high Mach number.

The spanwise vortices formed by the shearing of two supersonic flows rotate in the clockwise direction, as scaled by the dashed lines in Fig. 2(a). It is observed clearly that two neighboring vortices merge with each other. Due to the high-speed flow compressibility, the vortex is found to be compressed along the transverse direction, which results in an elliptic shape. Previous investigations have shown that the increase in flow compressibility leads to the decrease in shear layer thickness and the decrease in mixing efficiency.[30] From the point view of vortex dynamics in this study, the vortex becomes narrow in the transverse direction, and hence, the entrainment of free streams tends to be weak and the mixing region is reduced. As shown by the density-gradient contours in Fig. 2(a), the shocklets are characterized as the white-color stripes around the spanwise vortex. In particular, as the flow traverses the eddy shocklets, it is found that its density increases and the Mach number decreases, as depicted in Figs. 2(b) and 2(c). There are intense variations of density and Mach number in the supersonic shear layer. The eddy shocklets are formed randomly associated with the clockwise rotation of vortices, and the shocklets mainly distribute in the high-strain vortex-braid regions between two adjacent eddies. The high-speed flow compressibility can result in a strong spatial intermittency during the flow dilatation. In addition, the effects of flow compressibility lead to the partial recovery of the free-stream kinetic energy to the thermal energy as the fluid reaches the nearly stagnant central zone in the shear layer. As shown in Fig. 2(d), the local gas temperature is found to increase maximally by around a factor of 1.3, compared with the inflow static temperature T_A. Hence, it could be concluded that the increase in temperature from the combustion in the supersonic flow has a large component that is due to the effects of flow compressibility. It is also observed that the high-speed flow compressibility results in the alternating spatial distributions of expansion zones with low temperature/pressure and compression zones with high temperature/pressure in the shear layer. These unsteady features could have an influence on the dispersion and evaporation of droplets and will be analyzed in the following part.

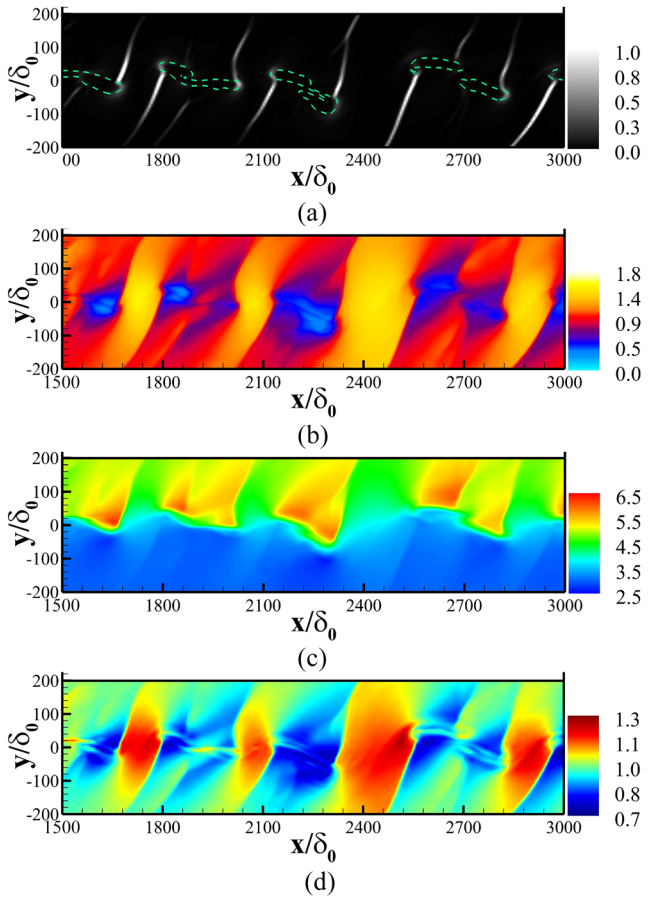

FIG. 2. Instantaneous contours of (a) density-gradient modulus normalized with the maximum value $|\nabla\rho|/|\nabla\rho|_{max}$ [green dashed lines for the dimensionless spanwise vorticity $\Omega_z/(\Delta U_A/\delta_0) = -0.01$], (b) dimensionless density ρ/ρ_A, (c) Mach number, and (d) dimensionless temperature T/T_A.

B. Segregation and evaporation of droplets

Figure 3 shows the instantaneous distribution of dispersed droplets with the temperature after the random release of the droplets from the inlet of the high-speed air stream. The fuel droplets

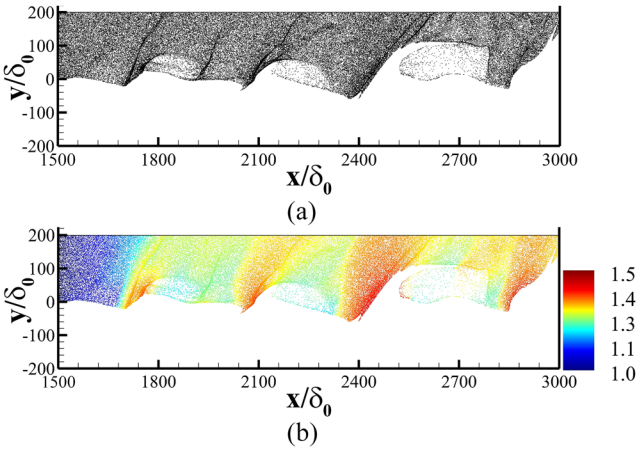

FIG. 3. Instantaneous distributions of the dispersed droplets (a) and the dimensionless droplet temperature T_d/T_{d0} (b).

disperse under the transportation of the large-scale vortex in shear layers. It is found that the droplet dispersion is closely related to the entrainment motion of the vortex. The droplets rotate clockwise around the vortex, associated with the clockwise rotational motion of the vortex. It can be observed that the droplets tend to segregate in the high-strain vortex-braid regions between two neighbor vortices and the periphery of the vortices. These phenomena are similar with the preferential segregation of droplets in low-speed incompressible flows. The difference is that in the highly compressible shear layer with shocklets, there are strip-shaped accumulation regions of droplets in the high-strain vortex-braid regions between the neighbor vortices, and the distribution pattern is found to be similar with the shape of shocklets.

In particular, Fig. 3(b) presents the contours of dimensionless droplet temperature (T_d/T_{d0}). Due to the high-speed flow compressibility, the local high temperature zones are found to be located in the high-strain regions between the large eddies, as shown in Fig. 2(b). Therefore, the droplets are heated by the local high-temperature air when they disperse into these high temperature zones and the droplet temperature rises. In addition, the high ambient pressure in the high-strain regions results in the increase in the boiling point of liquid, compared with that at the normal pressure. The associated increase in the wet bulb temperature causes the droplets to reach a higher temperature. In addition, it is found that the low ambient temperature in the vortex core cools the droplets that are entrained inside the vortex.

Figure 4 shows the instantaneous distributions of the fuel vapor mass fraction ($Y_F/Y_{F,max}$) at the same time with Fig. 3, which is found to have a direct relationship with the distribution patterns of the fuel droplets. The fuel vapors are found to be enriched in the high-strain regions between the vortices as well as the periphery of the vortices and are also concentrated as strip patterns outside the vortices. These features are due to the preferential segregation of droplets in the highly compressible shear layers with eddy shocklets. Therefore, the high-speed flow compressibility results in a more significant preferential accumulation of droplets, which affects the local enrichment of fuel vapors from droplet evaporation. This will, in turn, have an influence on the local mixing between the fuel and oxidant and further the ignition and combustion characteristics.

C. Instantaneous characteristics of heat and mass transfer

The aforementioned analysis focuses on the dispersion and evaporation features of sprayed droplets in the highly compressible shear layer flow. The following part will discuss the instantaneous features of the heat and mass transfer for an individual droplet from the sprayed droplets.

The high-speed compressibility in the supersonic flows can influence the heat and mass transfer during the droplet evaporation process due to the effects of flow compressibility on the ambient gas. For comparison, the heat and mass transfer process of a single droplet in the supersonic laminar flow is simulated as a comparison. The laminar flow case has the same aerothermodynamics conditions (velocity, pressure, and temperature) with those of the high-speed side of the present shear layer. Accordingly, the shearing vortices and the associated high-speed compressibility effects did not occur in the supersonic laminar flow. The initial velocity for the single droplet in the two cases equals to U_{A1} (the velocity of the high-speed air stream in the shear layer), and the initial temperature is 298.15 K. The evaporating droplet in the shear flow is released from the inlet of the high-speed side of air streams, and the droplets in the laminar flow are released in the flow with velocity U_{A1}. Figure 5 shows the evolution of the square of the droplet diameter. It is observed that the surface area of the droplets in the shear flow is reduced faster than that in the laminar flow. From the consideration of fluid dynamics, it is mainly because in the shear flow, the entrainment process of vortex results in the local low-speed region between the neighbor vortices, and the high-speed compressibility causes the gas in the low-speed region to have a higher temperature. These flow features, on the one hand, prolong the residence time of the droplet in the shear flow, and on the other hand, the heat transferred from the local high-temperature gas promotes the evaporation of the droplet.

According to the mass transfer equation (11) for a single droplet, it is found that there are two predominant physical parameters that determine the evaporation rate. The first one is the mass transfer coefficient B_m that scales the effects of the ambient environment on mass transfer when there is no convection on the droplet surface. The second one is the Sherwood number (Sh), which characterizes the effects of convection on the mass transfer. In general, the larger the values of these two physical quantities, the faster the mass transfer rates. Figure 6 presents the variations of these

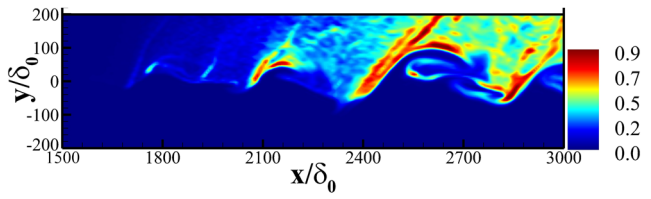

FIG. 4. Instantaneous distributions of the dimensionless fuel vapor mass fraction normalized with its maximum value $Y_F/Y_{F,max}$.

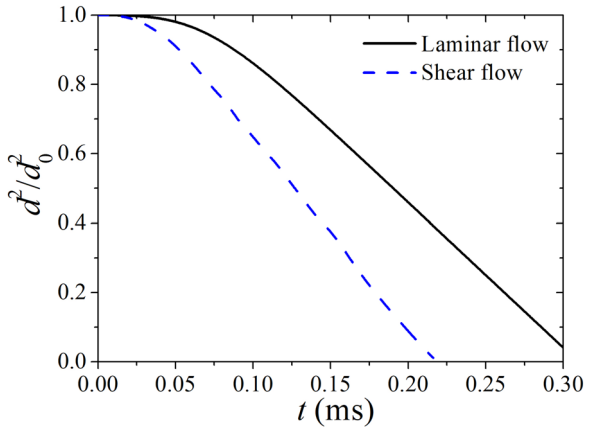

FIG. 5. Evolution of the dimensionless values of the square of the droplet diameter in laminar and shear flows.

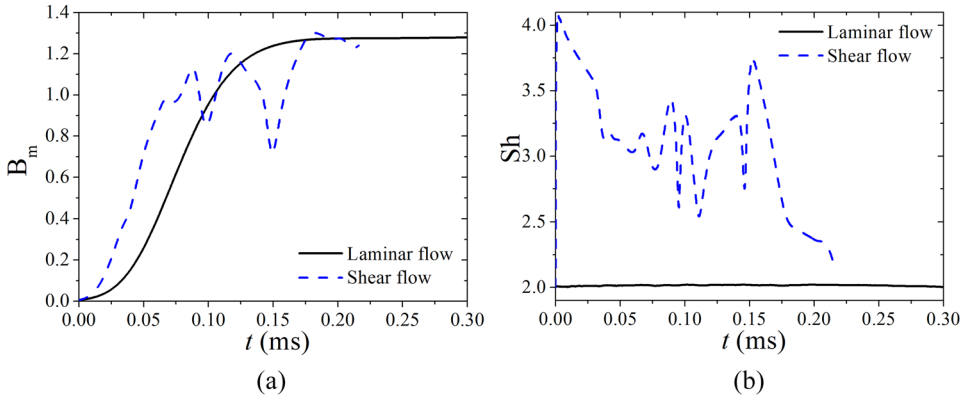

FIG. 6. Variations of the mass transfer number B_m (a) and the Sherwood number Sh (b) during the evaporation of droplets.

two parameters during the evaporation process starting from the release of the droplets. It is observed that the values of B_m and Sh in the shear layer flow is generally larger than those in the laminar flow. As the droplet is heated to evaporate in the laminar flow until they reach saturation, the mass transfer coefficient B_m first increases and then tends to become constant, as shown in Fig. 6(a). While there is a large fluctuation of B_m during the droplet evaporation process in the shear layer flow, this is due to the fact that the droplet undergoes the vortex cores with low temperature/pressure and the vortex braids with high temperature/pressure. The convection on the droplet surface is found to promote the mass transfer, as depicted in Fig. 6(b). In the laminar flow, there is no slip velocity between the droplet and the surrounding flow, and Sh remains unchanged with a value equaling two. In the shear layer, the vortices surrounding the droplet rotate with a change of local gaseous velocity. However, the inertia of the droplet causes it to have a delayed response to the velocity change of the surrounding gas. Therefore, there is the local velocity slip between the two phases, and the convection effect is prominent, which promotes the mass transfer.

The instantaneous mass transfer characteristics of the droplet in the above shear layer is analyzed in detail below. The ratio of the gas pressure seen by the droplet at the current moment to that at the previous moment, $P_g^{t+\Delta T}/P_g^t$, is used as the wave indicator for the determination of the compression wave (shocklets between the vortices) or the expansion wave (within vortices) at the current droplet position. Accordingly, when $P_g^{t+\Delta T}/P_g^t$ is larger than unity, it refers to a compression wave, and there is an expansion wave when $P_g^{t+\Delta T}/P_g^t$ is smaller than unity. As shown in Fig. 7, the droplet experiences two relatively strong compression waves from the release to the completion of evaporation. In particular, the cold droplet enters the hot gas stream and reaches the saturation state after an initial temperature rise. As the droplet passes through the first compression wave, the gas temperature seen by the droplet is increased obviously. The droplet responses to the increase in the ambient gas temperature and the temperature of droplet increase accordingly. Then, the droplet traverses the expansion wave downstream, and the gas temperature seen by the droplet decreases rapidly. The droplet responds to the cooling of the surrounding gas with a delayed process, since it has not finished the response to the upstream temperature rise. After that, the droplet passes through the second compression wave and the droplet temperature increases with the increase in the ambient gas temperature.

Theoretically, the high temperature gas in the compression wave region could promote the mass transfer from the droplet to the ambient gas. However, the present analysis cannot demonstrate these features. In the following part, the transient variations of B_m and Sh as the droplet traverses the compression and expansion waves will be analyzed in detail to explain these phenomena.

Figure 8 shows the instantaneous variations of B_m and Sh during the droplet evaporation in the shear layer. When the droplet undergoes the compression wave affecting region, the mass transfer coefficient, B_m, decreases and hence the mass transfer is suppressed. In the expansion affecting region, B_m increases and the mass transfer is enhanced accordingly. In particular, the droplet temperature increases as the droplet traverses the compression wave. However, the gaseous pressure seen by the droplet rises simultaneously and suppresses the evaporation due to the decrease in B_m. Therefore, the combined influence of the variation of ambient pressure and temperature results in the decrease in B_m, associated with the suppression of mass transfer. It is observed that B_m increases first and

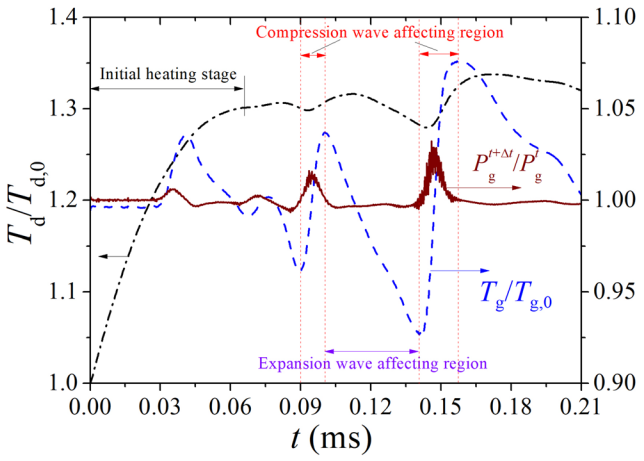

FIG. 7. Evolution of the droplet temperature and the gas temperature seen by the droplet during the evaporation in the shear layer.

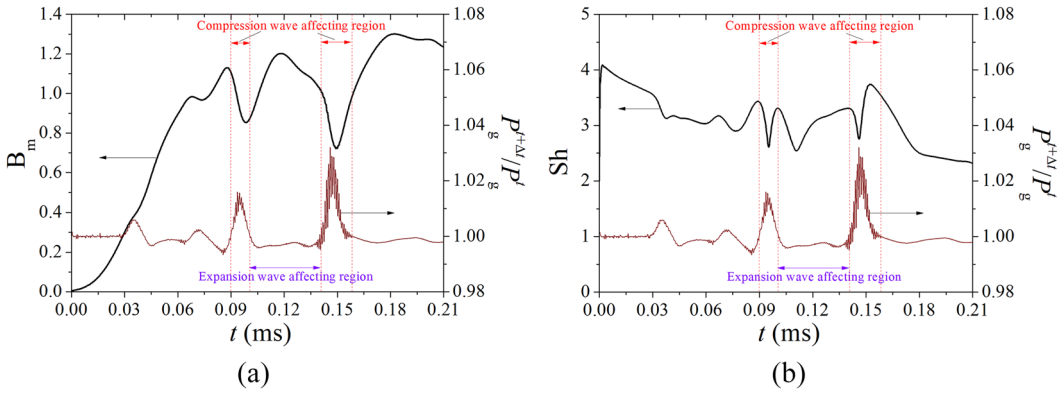

FIG. 8. Evolution of mass transfer number B_m (a) and Sherwood number Sh (b) during the evaporation of the droplet in shear layers.

then decreases during the droplet traversing in the expansion wave region. For the initial increase, it is because, on the one hand, the gas pressure in the expansion wave region decreases, and on the other hand, the droplet does not finish the response to the gas temperature rise from the upstream compression wave. The delayed response results in the continuous increase in the droplet temperature as well as the increase in B_m. The reason for the subsequent decrease in B_m is that the droplet completes the response of the gas temperature rise in the upstream compression zone, and then, the droplet responds to the gas temperature decrease from the current expansion wave, associated with the decrease in the droplet temperature. In general, the evaporation process occurs in which B_m increases first and then decreases during the droplet traversing in the expansion wave region.

For the variations of the Sherwood number, concerning the convection effects on the mass transfer, it is found that Sh decreases first and then increases both in the compression wave regions and in the expansion wave region. In particular, as the droplet traverses the first compression wave, the gas velocity seen by the droplet decreases obviously and there is an expansion wave region before passing through the first compression wave, associated with the increase in the gas velocity seen by the droplet. The droplet has not finished the response to the velocity increase in the upstream expansion region as it traverses the first compression wave, and hence, the droplet velocity decreases but the ambient gas velocity increases in the first compression wave region. After the droplet completes the response to the gas velocity increase from the upstream expansion wave, it starts to respond to the decrease in gas velocity in the first compression wave region. Therefore, the slip velocity of the two phases is first decreased and then is increased in the compression wave region. The droplet has a similar velocity response characteristic as it traverses the second compression wave. During the droplet traversing of the expansion wave between the two compression waves, the droplet still responds to the decrease in gas velocity from the upstream compression wave, and hence, the droplet velocity decreases but the gas velocity seen by the droplet increases. Consequently, the slip velocity is found to be decreased first and then increased, resulting in the evolution features of the Sherwood number in the compression wave and the expansion wave regions.

IV. CONCLUSIONS

In this research, the preferential concentration and evaporation of fuel droplets in spatially developing supersonic shear layers with high flow compressibility are studied. The numerical approximation of the spatial derivatives of the physical quantities is achieved by a sixth-order hybrid WENO scheme, and the dispersions of evaporating droplets are tracked as point mass. The fluid quantities seen by the droplets are calculated via a fourth-order Lagrangian polynomial interpolation method. Two-way interactions for the mass, momentum, and energy between the liquid and gas phases are modeled into the source terms of governing equations in the Eulerian frame.

The droplets are found to preferentially segregate in the vortex-braids as well as the periphery of vortices, which is consistent with the accumulation features of droplets in incompressible flows with low compressibility reported previously. This is due to the fact that there exists the strongest interaction between the dispersing droplets and the vortices. When the droplets traverse the eddy shocklets in the shear layer with high compressibility, the droplets are decelerated in response to the velocity decrease of the surrounding gas, and there are obvious nonuniform distributions that the droplets segregate as stripes in the downstream region of the shocklets.

There are spatial alternating distributions of the high-temperature vortex-braid zones and the low-temperature vortex-core zones in the compressible shear layers with the high convective Mach number. The instantaneous analysis shows that the droplet has the relaxation response behaviors for the momentum and heat transfers from the surrounding carrier gas due to the droplet inertia, and it is found that the high-temperature environment in the vortex-braids cannot promote the mass transfer and the evaporation of the droplet significantly. On the contrary, the heat and mass transfers are enhanced to some extent when the droplet traverses the vortex-core regions with low-temperature and low-pressure.

It should be emphasized that the present research mainly considers the preferential segregation and evaporation of droplets in the nonreacting supersonic shear flow with high compressibility. The ignition and flame features are worth for further investigation due to the importance for the supersonic combustion in scramjets. The results and conclusions presented in this research might

provide some new insights into the transportation, dispersion, and evaporation of fuel droplets in supersonic flows and combustion.

ACKNOWLEDGMENTS

This research was partially supported by the National Natural Science Foundation of China (Grant Nos. 51676111, 51806179, and NSAF.U1730104), the project funded by the China Postdoctoral Science Foundation, the Fundamental Research Funds for the Central Universities, and the National Science and Technology Major Project (No. 2017-III-0005-0030).

REFERENCES

[1]S. Balachandar and J. K. Eaton, "Turbulent dispersed multiphase flow," Annu. Rev. Fluid Mech. **42**, 111–133 (2010).
[2]S. Lee, S. K. Lele, and P. Moin, "Eddy shocklets in decaying compressible turbulence," Phys. Fluids A **3**(4), 657–664 (1991).
[3]E. Balkovsky, G. Falkovich, and A. Fouxon, "Intermittent distribution of inertial particles in turbulent flows," Phys. Rev. Lett. **86**(13), 2790 (2001).
[4]F. Toschi and E. Bodenschatz, "Lagrangian properties of particles in turbulence," Annu. Rev. Fluid Mech. **41**, 375–404 (2009).
[5]H. Kada and T. J. Hanratty, "Effects of solids on turbulence in a fluid," AIChE J. **6**(4), 624–630 (1960).
[6]B. J. Lazaro and J. C. Lasheras, "Particle dispersion in a turbulent, plane, free shear layer," Phys. Fluids A **1**(6), 1035–1044 (1989).
[7]F. Wen, N. Kamalu, J. N. Chung *et al.*, "Particle dispersion by vortex structures in plane mixing layers," J. Fluids Eng. **114**(4), 657–666 (1992).
[8]E. K. Longmire and J. K. Eaton, "Structure of a particle-laden round jet," J. Fluid Mech. **236**, 217–257 (1992).
[9]E. Calzavarini, T. H. van den Berg, F. Toschi *et al.*, "Quantifying microbubble clustering in turbulent flow from single-point measurements," Phys. Fluids **20**(4), 040702 (2008).
[10]J. Bec, L. Biferale, M. Cencini *et al.*, "Heavy particle concentration in turbulence at dissipative and inertial scales," Phys. Rev. Lett. **98**(8), 084502 (2007).
[11]Q. Wang and K. D. Squires, "Large eddy simulation of particle-laden turbulent channel flow," Phys. Fluids **8**(5), 1207–1223 (1996).
[12]P. Gualtieri, F. Picano, and C. M. Casciola, "Anisotropic clustering of inertial particles in homogeneous shear flow," J. Fluid Mech. **629**, 25–39 (2009).
[13]M. S. Dodd and A. Ferrante, "On the interaction of Taylor length scale size droplets and isotropic turbulence," J. Fluid Mech. **806**, 356–412 (2016).
[14]S. Lee, S. K. Lele, and P. Moin, "Direct numerical simulation of isotropic turbulence interacting with a weak shock wave," J. Fluid Mech. **251**, 533–562 (1993).
[15]S. Pirozzoli and F. Grasso, "Direct numerical simulations of isotropic compressible turbulence: Influence of compressibility on dynamics and structures," Phys. Fluids **16**(12), 4386–4407 (2004).
[16]M. Samimy and S. K. Lele, "Motion of particles with inertia in a compressible free shear layer," Phys. Fluids A **3**(8), 1915–1923 (1991).
[17]F. Mashayek and F. A. Jaberi, "Particle dispersion in forced isotropic low-Mach-number turbulence," Int. J. Heat Mass Transfer **42**(15), 2823–2836 (1999).
[18]P. Olla, "Preferential concentration versus clustering in inertial particle transport by random velocity fields," Phys. Rev. E **81**(1), 016305 (2010).
[19]Y. Yang, J. Wang, Y. Shi *et al.*, "Interactions between inertial particles and shocklets in compressible turbulent flow," Phys. Fluids **26**(9), 091702 (2014).
[20]Q. Zhang, H. Liu, Z. Ma *et al.*, "Preferential concentration of heavy particles in compressible isotropic turbulence," Phys. Fluids **28**(5), 055104 (2016).
[21]A. Burcat and B. Ruscic, "Third millenium ideal gas and condensed phase thermochemical database for combustion (with update from active thermochemical tables)," Report No. ANL-05/20, Argonne National Laboratory, Argonne, IL, USA, 2005.
[22]B. E. Poling, J. M. Prausniz, and J. P. O'Connell, *The Properties of Gases and Liquids* (McGraw-Hill Chaps, New York, 2001), pp. 10–11.
[23]R. S. Miller, K. Harstad, and J. Bellan, "Evaluation of equilibrium and non-equilibrium evaporation models for many-droplet gas-liquid flow simulations," Int. J. Multiphase Flow **24**(6), 1025–1055 (1998).
[24]Z. Ren, B. Wang, Q. Xie *et al.*, "Thermal auto-ignition in high-speed droplet-laden mixing layers," Fuel **191**, 176–189 (2017).
[25]Z. Ren, B. Wang, and L. Zheng, "Numerical analysis on interactions of vortex, shock wave, and exothermal reaction in a supersonic planar shear layer laden with droplets," Phys. Fluids **30**(3), 036101 (2018).
[26]X. Y. Hu, Q. Wang, and N. A. Adams, "An adaptive central-upwind weighted essentially non-oscillatory scheme," J. Comput. Phys. **229**(23), 8952–8965 (2010).
[27]Y. Zhang, B. Wang, H. Zhang *et al.*, "Mixing enhancement of compressible planar mixing layer impinged by oblique shock waves," J. Propul. Power **31**(1), 156–169 (2014).
[28]T. J. Poinsot and S. K. Lelef, "Boundary conditions for direct simulations of compressible viscous flows," J. Comput. Phys. **101**(1), 104–129 (1992).
[29]J. O'Brien, J. Urzay, M. Ihme *et al.*, "Subgrid-scale backscatter in reacting and inert supersonic hydrogen–air turbulent mixing layers," J. Fluid Mech. **743**, 554–584 (2014).
[30]B. Wang, W. Wei, Y. Zhang *et al.*, "Passive scalar mixing in $M_c < 1$ planar shear layer flows," Comput. Fluids **123**, 32–43 (2015).